RSC Advances

ROYAL SOCIETY OF CHEMISTRY

www.rsc.org/advances

Investigation of thermal decomposition and stability of energetic 1, 2, 4-Triazole derivatives using UV laser based pulsed photoacoustic technique

K. S. Rao, and A.K. Chaudhary *

Advanced Centre of Research in High Energy Materials, University of Hyderabad, Hyderabad-500 046, India

Email: anilphys@yahoo.com , akcphys@gmail.com

Abstract: This paper is in continuation of our previous report which was based on 532 nm wavelength pulsed photoacoustic (PA) technique of nitro rich energetic materials named 1-(4-Methyl-3,5-dinitrophenyl)-1H-1,2,4-triazole(*P*-Me-DNPT),1-(4-Methoxy-3,5-dinitrophenyl) -1H-1,2,4-triazole (*P*-OMe-DNPT), 2,6-Dinitro-4-(1H-1,2,4-triazol-1-yl) aniline (*P*-NH_2-DNPT) between 30-350 ^oC temperature range [1]. In the present work, the PA fingerprint spectra, thermal stability and efficiency of these compounds as rocket fuel have been evaluated using fourth harmonic i.e. 266 nm wavelength of 7 ns pulse duration and 10 Hz repetition rate as an excitation source. The entire study is based on photodissociation process due to $\pi^* \leftarrow n$ electronic transition in NO_2 molecules which is initiated inside the PA cell. The result obtained from PA technique and thermo gravimetric-differential thermal analysis (TG-DTA) data confirm the multistep decomposition mechanism. The study also provides the stable thermal quality factor "Q" which is linked to the stability of the compound.

Keywords: Thermal PA spectra, 266 nm, 1, 2, 4-1H-triazoles, stability, photoacoustic

1. Introduction

Triazoles and their derivatives have the advantage of high nitrogen content and density, good thermal stability, low impact sensitivity and high explosive volume, less molecular weight, because of which they can be used both for civil and military applications such as explosives, propellants and pyrotechnics [2,3]. Researchers have made continuous efforts to develop new high energy materials (HEMs) having good thermal stability, impact and shock insensitivity, good performance, and environmental friendly syntheses for future military and space applications [4,5]. Several groups have focused on theoretical and experimental studies to understand the thermal decomposition (TD) mechanism and stability criteria of different types of energetic 1, 2, 4-triazoles [6-13]. Zhang Rui-Zhou *et al.* reported theoretical studies on a series of 1,2,4-triazoles derivatives as potential high energy density compounds [2]. The decomposition mechanism of other HEMs molecules can be studied using different types of analytical techniques [14-21].

Tagomori *et al*. examined the thermal decomposition mechanism of 1H-1,2,4-triazole (1Htri) and its derivatives with different substituent such as $-NO_2$, $-NH_2$, $-CH_3$, $-OCH_3$ and -COOH using sealed-cell differential scanning calorimetry (SC-DSC) [6]. However, in the present case, the molecules 1, 2, 4-triazoles have identical structures with different chemical substituent such as $-CH_3$, $-OCH_3$, and $-NH_2$ which are present at *para* position of phenyl ring. The role of these substituent was investigated during the process of thermal decomposition between the temperature range of 30-350 ^oC using pulsed photoacoustic pyrolysis technique. The released quantity of gaseous products was measured in terms of the strength of PA signal, which depends on the density of compounds.

The PA technique works on the principle of detection of acoustic pressure wave generated by HEMs vapor after absorption of incident laser radiation of suitable wavelengths. It is well known that the vapor of HEMs molecules and their byproducts have strong absorption in 266 nm wavelength range and are involved in photo dissociation process due to $\pi^* \leftarrow n$ transitions

[22,23,24]. The HEMs compounds release several byproduct gaseous molecules, such as NO_2, NO, CO_2, CO, HCN and H_2O in the process of thermal decomposition. In our earlier reports, we have investigated thermal decomposition of a different type of HEMs from triazole derivatives of benzyl and phenyl series using pulsed PA technique and established that NO_2 is one of the principal byproduct gases [1, 25, 26]. For this study 532 nm wavelength was used as an excitation source. However, when we select 266 nm as an excitation wavelength, the study of thermal decomposition is shifted to total compound vapor. Several research groups reported that laser-based excitation is responsible for reduction of activation barriers for decomposition reactions [22,27,28]. Kimmel .et al suggested the dynamics and steady roots of TD mechanism of HEMs molecules with NO_2 and NO as byproducts [29]. Several research groups reported that NO_2 molecules photo dissociated to NO in presence of ultraviolet (UV) radiations [30-35]. It is also known that NO_2 is one of the principal byproduct gas obtained during the decomposition of HEMs compounds. Therefore, NO_2 molecules follow the root of photo dissociation (inside the PA cell) and converted into NO in presence of UV light (i.e. in present case 266 nm). The root of photo dissociation is shown in Eq (1):

$$NO_2 + h\nu \rightarrow NO + O \quad (1)$$

Therefore, it is inferred that the major contribution to PA signal due to NO molecules. In the present case, the thermal stability of the reported compounds was examined based on 266 nm wavelengths and the study helps us to ascertain the efficiency of these compounds as a rocket fuel.

Kommu et al reported the synthesis of present studied compounds labeled as *P*-Me-DNPT, *P*-OMe-DNPT and *P*-NH_2-DNPT [36]. The estimated values of densities are 1.62, 1.64, and 1.66 g/cm^3; respectively. Fig. 1(a-c) shows the line-bond structures of these compounds. These molecules have similar structures with difference in their principal functional group occupied at *para* position of phenyl ring. The *para* position is replaced by -CH_3, -OCH_3 and -NH_2

groups. Therefore, these compounds release homogeneous mixture of NO_2 and other gaseous products during thermal decomposition. The selection of 266 nm as an excitation wavelength provides the signature of the compounds in terms of generated PA signal for the given PA cell.

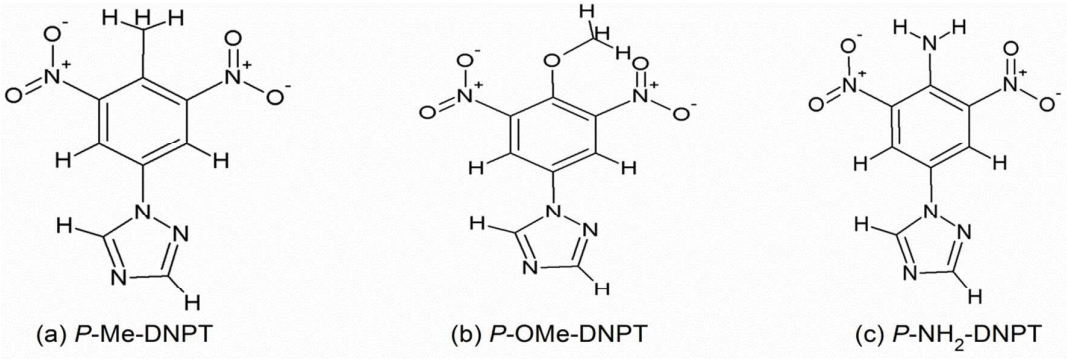

Fig. 1. Line-bond strutures of (a) *P*-Me-DNPT, (b) *P*-OMe-DNPT, and (c) *P*-NH_2-DNPT.

2. Experimental Arrangements

The experimental set up used in the laboratory is shown in Fig. 2. The PA cell, which was used in the experiment to record the thermal PA spectrum, was made up of stainless steel. It has internal diameter of 1.5 cm and length of 7.5 cm. The quartz windows were placed on both sides of the cell to allow laser radiation. Solid HEMs compounds (~1.0 mg) were placed in a round bottom flask for controlled pyrolysis between 30 and 350 ^{o}C range. A needle valve was used to control the rate of flow of vapor through the inlet. The photoacoustic signal (PA signal) produced by the vapor is detected by pre-polarized microphone of responsivity 50 mV/Pa (BSWA, China). The output signal of the microphone was fed to the preamplifier, which was coupled to the 200 MHz oscilloscope (Tektronix, U.S.A). The output signal of oscilloscope was then connected to a personal computer, which has LabView software installed to carry out the data analysis.

The melting and decomposition temperatures of samples are measured by Thermo Gravimetric-Differential Thermal Analysis (TG-DTA instrument: Model No. Q600DT). The

solid compound was introduced into an alumina crucible and heated between 25-400 ^{o}C temperature range under nitrogen gas atmosphere (flow rate of 100 cm^{3} / min) which works as the purge and protective gas. Non-isothermal TGA runs were conducted between 25-400 ^{o}C range in nitrogen atmosphere with purge rate of 10 ^{o}C /min. In addition, FTIR spectra were obtained in dichloromethane solution using a JASACO FT/IR- 5300 spectrometer in the region of 400-4000 cm^{-1}.

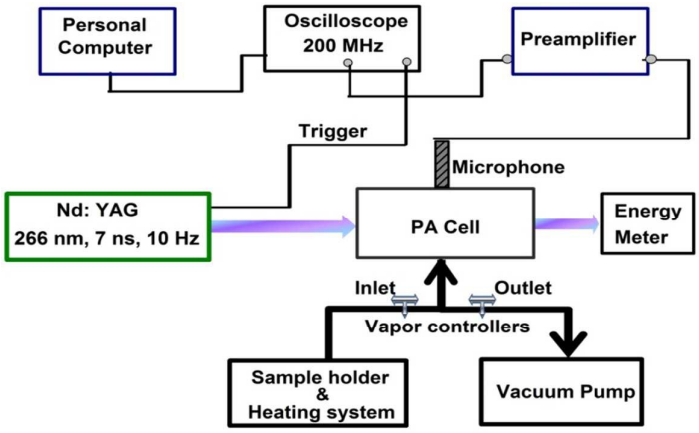

Fig. 2. Experimental set up.

3. Results and discussions

3.1. FTIR spectra

Fig. 3(a-c) shows the FTIR spectra of compounds recorded in dichloromethane solution. Inset tables show the wave number range of the corresponding functional groups. In addition, inset images show the chemical molecular structure of the compounds.

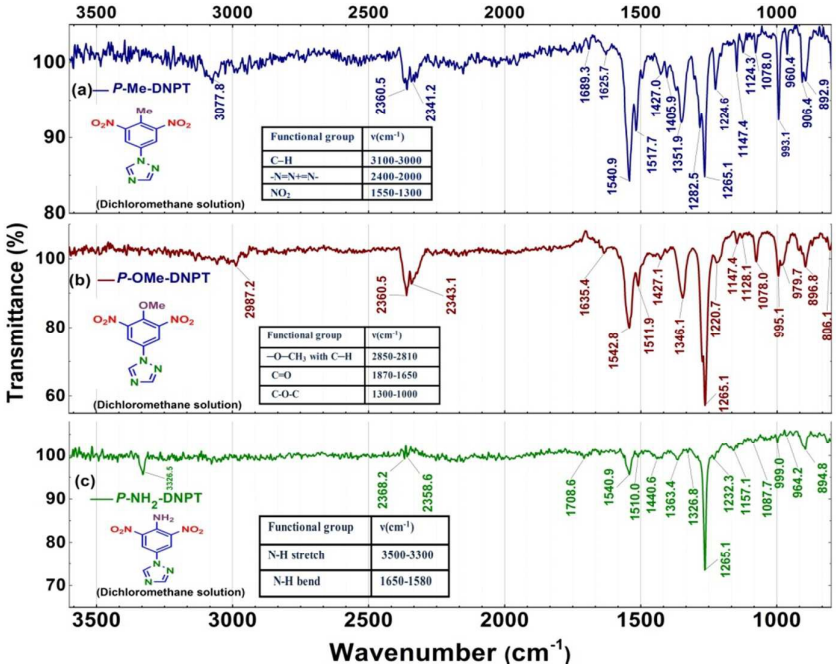

Fig. 3 IR spectra of (a) *P*-Me-DNPT (b) *P*-OMe-DNPT and (c) *P*-NH_2-DNPT.

3.2. Thermal PA fingerprint spectra of compounds

Fig. 4(a-c) shows the thermal PA spectra of *P*-Me-DNPT, *P*-OMe-DNPT and *P*-NH_2-DNPT, respectively. The PA spectra were recorded between 40-350 ^oC range, at E_{in} = 10 μJ and t = 0.5 ms. The HEMs vapor and its dissociation fragments such NO_2, NO, CO, CO_2, HCN and H_2O etc. have strong absorption at 266 nm wavelength. Therefore, very low incident laser energy of the order of 10 μJ is sufficient to generate a strong PA signal. The PA spectra of these compounds have similar excited acoustic modes located at 3.8, 8.4, 13.8, 27.8 and 38.8 kHz, respectively. The central frequency of acoustic modes varies from compound to compound. Whereas, it remain unchanged as a function of temperature for each compound. This indicates that compounds release similar type of gaseous mixture during their decomposition process between the 40-350 ^oC temperature range. The central frequencies of acoustic modes have shifted to ± 200 Hz from one to another compound.

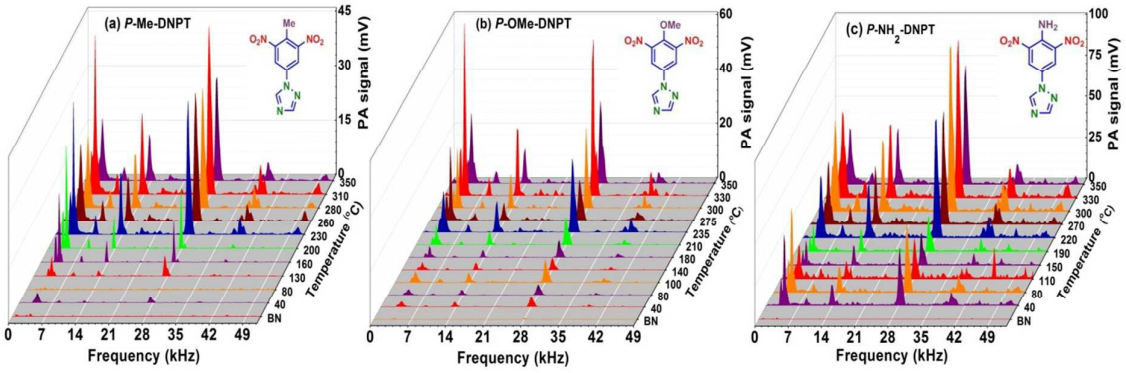

Fig. 4. Temperature based PA spectra of (a) *P*-Me-DNPT, (b) *P*-OMe-DNPT and (c) *P*-NH_2-DNPT.

Fig. 4(a-c) exhibits the significance of PA signal obtained at initial temperature i.e. 40 ^oC. This supports our earlier findings that NO_2 released before melting temperature [37,38]. Also, the molecules vapor has strong absorption at 266 nm, which are released after melting temperature. However, before melting temperature only NO_2 is released in low quantity as a result small PA signal is obtained at 40 ^oC. The PA signals of *P*-Me-DNPT, *P*-OMe-DNPT and *P*-NH_2-DNPT become more intense after crossing the temperatures of 130, 180 and 190 ^oC respectively. Before reaching these temperatures, the compounds exhibit constant PA signal, which clearly indicates their thermal stability. The maximum strength of PA signal is obtained above the decomposition temperatures i.e. at 310 ^oC for *P*-Me-DNPT, 330 ^oC - *P*-OMe-DNPT and 300 ^oC for *P*-NH_2-DNPT. However, the decomposition temperature of these compounds lies near to 270 ^oC, the exact values of as shown in Fig. 5(d,e,f) are present at 260, 275 and 270 ^oC, respectively. The maximum strength of PA signals obtained for the compound is in following order: *P*-NH_2-DNPT > *P*-OMe-DNPT > *P*-Me-DNPT. Due to the presence of -NH_2 group, *P*-NH_2-DNPT has higher density, which leads to release the high quantity of gaseous mixture (provides higher strength of PA signal) than the other compounds. Many researchers have shown that N-NO_2 and C-NO_2 bonds are the weakest bond in energetic ring and the rupture of these bonds is the first step of the decomposition process [39,40,41]. In the present case, the chemical substituent -NH_2 and -OCH_3 increase the

density of compounds than -CH_3 and lead to the release of initially NO_2 molecules which is followed by other gaseous byproducts during the pyrolysis process between 30-350 ^oC, range. The results obtained from PA technique reveal that higher concentrations of gaseous molecules are released from *P*-NH_2-DNPT and *P*-OMe-DNPT as compared to *P*-Me-DNPT. Therefore, N, O, and NO_2 rich triazole derivatives are potential interesting energetic compounds due to high density, energy and properties as solid propellants and explosives [42].

3.3. Thermal stability of the compounds and their efficiency as a rocket fuel

Fig. 5(a-c) shows the behavior of excited acoustic modes with respect to temperature, while, Fig. 5(d-f) exhibits the TG-DTA thermo graphs. Fig. 5(a) shows the intensity of excited acoustic modes for *P*-Me-DNPT possess constant in nature between 40-130 ^oC range. This also confirms that the compound releases same concentration of gaseous fragments. However, with further increase in vapor temperature, the PA signal shows growth and has two maximum peaks, which are present at 230 and 310 ^oC respectively. These peaks also indicate that thermal energy is released in multiple steps, confirming that stepwise decomposition process of *P*-Me-DNPT. All the acoustic modes show similar behavior with variation in their predominant order with respect to temperature. The heat flow curve of *P*-Me-DNPT has two endothermic peaks as shown in Fig. 5(d), which indicates that the compound has melting, and decomposition temperatures at 129.80 ^oC, 259.89 ^oC, respectively. The HEMs compounds possess solid-solid phase transition at the melting temperature, therefore the heat flow curve shows endothermic peak. However, the ring breaking reactions at decomposition temperature show either endothermic or exothermic in nature. Due to the lack of high nitrogen content in *P*-Me-DNPT, it shows endothermic peak at its decomposition temperature. The weight loss curves show that *P*-Me-DNPT is thermally stable up to 150 ^oC, which lost 95 % of its total weight between 150-235 ^oC, range.

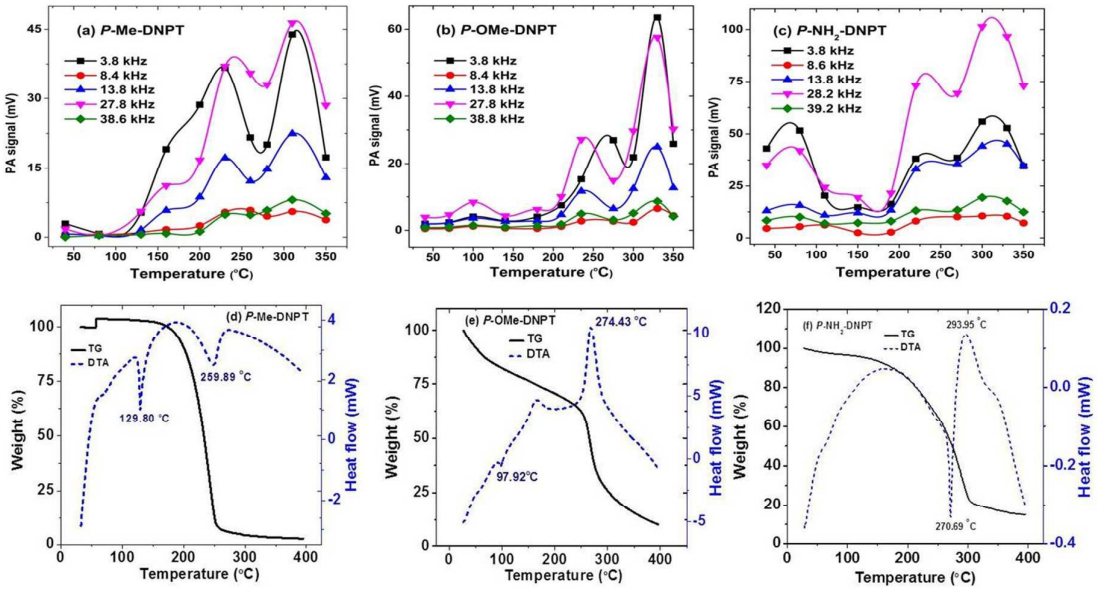

Fig. 5. Behavior of acoustic modes and TG-DTA curves of compounds.

Fig. 5(b) depicts that *P*-OMe-DNPT releases nearly similar quantity of gaseous molecules between 40-210 ^{o}C, range. However, the PA signal curves has slightly high intensity near the melting temperature i.e. 100 ^{o}C (97.92 ^{o}C). The intensity of acoustic modes is high at the temperatures 235 and 330 ^{o}C. Fig. 4(e) shows the TG-DTA curves of *P*-OMe-DNPT. It has melting and decomposition temperatures at 97.92 and 274.43 ^{o}C, respectively. The weight loss curve indicates that the compound decomposes gradually between 25-275 ^{o}C, range.

Fig. 5(c) depicts the behavior of acoustic modes with respect to temperature for *P*-NH_2-DNPT. The intensity of acoustic modes at 8.4, 18.8 and 38.8 kHz does not show any variation between 40-190 ^{o}C, range. While for predominant modes present at 3.8 and 28.2 kHz, the intensity is high at initial temperature. However, all the acoustic modes possess maximum intensity at 220 and 300 ^{o}C. The heat flow curve as shown in Fig. 5(f) exhibits that the compound *P*-NH_2-DNPT has common melting and decomposition temperature at 270 ^{o}C. The process of melting initiates at 180 ^{o}C and decomposed at 270 ^{o}C. However, heat flow curve exhibits exothermic nature at 293 ^{o}C [43]. Therefore, this temperature can be treated as second decomposition temperature. Also, due to exothermic nature at this temperature, the released

gaseous concentration is high as a result the maximum strength of PA siganl is obtained. The weight loss curve shows that the compound is thermally stable upto 150 ^{o}C, it losses around 70 % of its total weight between 150-300 ^{o}C range. The results obtained form both techniques i.e. in terms of strengths of PA signal and weight loss during the decomposition process confirms the thermal stability of the compounds.

In addition, the efficiency of these compounds as a rocket fuel is found of the order of *P*-NH_2-DNPT > *P*-Me-DNPT > *P*-OMe-DNPT. This evaluation is based on the strength of PA signal obtained from PA spectra and residual weight measured from the TGA (weight loss) curve. The values of density (ρ), velocity of detonation (*D*), detonation pressure (*P*), initial weight (I_w), residual weight (R_w) obtained from TG-DTA data and maximum intensity of PA signal of the compounds are comprised in Table .1.

Table 1 The values of ρ, *D*, *P*, I_w, R_w and intensity of PA signal.

Compound	ρ (g/cm^3)	*D* (km/s)	*P* (GPa)	TG-DTA		PAS (mV)
				I_w (mg)	R_w (%)	*t* = 0.5 ms
P-Me-DNPT	1.62	6.40	17.01	1.589	3	46.42
P-OMe-DNPT	1.64	6.68	18.68	1.002	10	63.55
P-NH_2-DNPT	1.66	6.66	18.74	3.254	15	101.42

The compound *P*-OMe-DNPT shows less efficiency than that of *P*-Me-DNPT. Even though, it has highest PA signal, detonation pressure and velocities compared to *P*-Me-DNPT. Because, the measured residual weight is 10 % for the initial weight 1.002 mg. While, the residual weight is 3% for 1.589 mg of *P*-Me-DNPT. The compound *P*-OMe-DNPT having highest residual weight even for small quantity of initial weight, which indicates that *P*-OMe-DNPT is less efficient compound. However, all the solid compounds ~1.0 mg used in the controlled PA pyrolysis process. The compopund *P*-NH_2-DNPT possess highest density 1.66 g cm^{-3}, detonation pressure 18.74 GPa. Therefore, it releases high concentration of gaseous byproducts. Consequently, the strength of PA signal is higher as compared to other

compounds and indicates that it is much efficient material as a rocket fuel. However, its velocity of detonation is 6.66 km/s, while for *P*-Me-DNPT it is 6.40 km/s and *P*-OMe-DNPT has 6.68 km/s. The compound *P*-OMe-DNPT has high detonation velocity it might due presence of additional O atom. A high density is vital to the performance of an energetic material because the detonation pressure is proportional to the square of its density [44]. In our earlier report [1], thermal stability of these compounds was evaluated based on released quantity of NO_2, which depends on bond lengths of chemical substituent present in the compound. However, in the present case the total released vapor is responsible for the generation of acoustic signal. Therefore, the thermal stability of the compound is evaluated on the basis of released quantity of total vapor. The results obtained from the both reports confirms that photoacoustic technique is one of the emerging spectroscopic technique to examine the thermal stability, and decomposition mechanism of newly synthesized energetic materials and to scale their efficiency as a rocket fuels in terms of released quantity of gaseous molecules irradiated using suitable excitation wavelength.

However, the burning temperature of rocket fuels is more than 400 ^{o}C. Here, the compounds are directly burnt with oxidizers as a result the compounds release the end products of C-H-N-O [3]. Moreover, in the present experiment recording of PA signal above 400 ^{o}C is restricted due to the diaphragm of the microphone, which gets damaged at higher temperature. Therefore, the thermal stability and efficiency of HEMs compounds was evaluated between 30-350 ^{o}C range. We have already shown below flash point temperature range the molecules are releasing higher concentration of gaseous fragments, which can monitor in terms of strength of PA signals. Therefore, data obtained from photoacoustic and TG-DTA techniques below 400 ^{o}C range, the efficiency of the HEMs compounds can be evaluated.

3.4. Comparative study of PA fingerprints

The calculated frequencies of the given PA cell are listed in Table. 2. Fig. 6(a-c) shows the maximum strength of photoacoustic fingerprint spectra of title compounds recorded at 310, 300, and 330 ^{o}C, respectively. The inset figure shows the time signals recorded at incident laser energy E_{in} = 10 μJ and data acquisition time t = 1 ms. The excited acoustic modes (which have intensities higher than 1.0 mV) and corresponding intensities are comprised in Table. 3.

The structures of the compounds are similar except their major chemical substituent present at *para* position of phenyl ring. These compounds release similar type of gaseous mixture with different concentration. As a result, the compounds possess similar cavity modes with small shift in the frequency and they have different intensities. The intensity of acoustic modes are high for *P*-NH_2-DNPT, and also this compound has additional modes compared to other samples. It is clearly observed in Table 3, that the excited acoustic modes have small shift in their central frequencies from one sample to another sample.

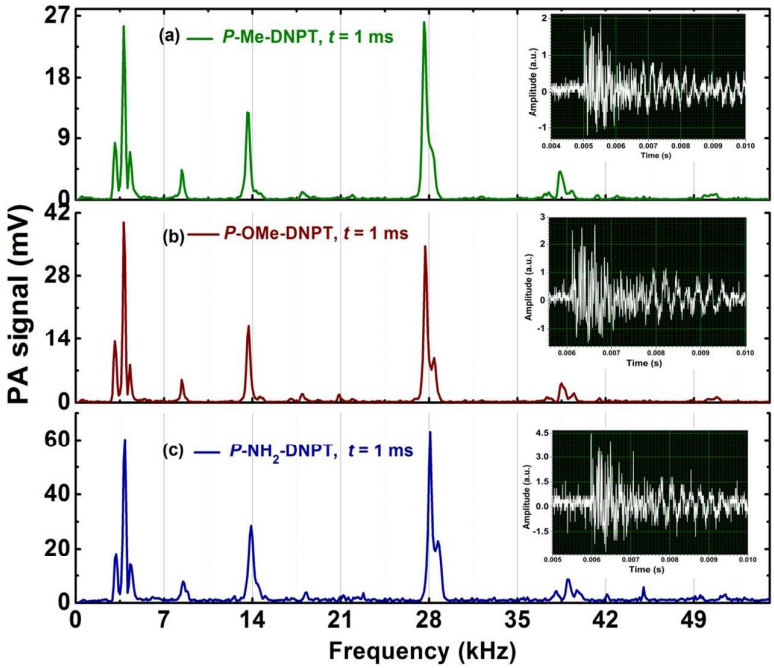

Fig. 6. PA fingerprint spectra at decomposition temperatures, t = 1 ms.

Table 2 Calculated frequencies of PA cavity.

Longitudinal *(q)*:	1	2	3	4	5	6	7	8	9	10	11
f (kHz) :	2.28	4.57	6.86	9.14	11.43	13.72	16.00	18.29	20.58	22.86	25.15
Longitudinal *(q)* :	12	13	14	15	16	17	18	19	20	21	22
f (kHz):	27.44	29.72	32.01	34.30	36.58	38.87	41.16	43.44	45.73	48.02	50.30

Radial (*n*) :	1	2	3	Azimuthal *(m)*:	1	2
f (kHz):	13.4	22.2	30.5	*f* (kHz):	27.89	38.8

Table 3 Excited acoustic modes and their intensities.

P-Me-DNPT	*f* (kHz) :	3.1	3.8	4.3	8.4	13.6	18	27.6	37.5	38.4	39.3					
	I (mV) :	8.3	25.5	6.9	4.4	12.9	1.1	26.1	1.1	4.2	1.3					
P-OMe-DNPT	*f* (kHz) :	3.1	3.8	4.3	8.4	13.7	18	20.9	27.7	28.4	38.5	39.5				
	I (mV) :	7.9	23.6	4.9	2.9	10.1	1.1	1.0	20.4	5.8	2.5	1.2				
P-NH_2-DNPT	*f* (kHz) :	3.2	3.9	4.3	8.5	13.9	18.3	21.2	22.8	28.1	28.7	38.1	39	39.7	42.1	45	51.5
	I (mV) :	18.2	60.3	14.1	7.8	28.5	3.8	2.8	3.6	63.2	22.9	4.3	9.5	4.7	3.1	5.7	3.1

The calculated frequencies of the PA cavity shows the first radial and azimuthal eigenmodes are overlapping with sixth and twelfth longitudinal modes, respectively. These are the predominant modes in PA spectra of compounds occupied at 13.8 and 27.8 kHz, respectively.

3.5. Effect of data acquisition time

Fig. 7(a-c) depicts the PA spectra of compounds while Fig. 7(d-f) shows the behavior of excited acoustic modes with respect to the data acquisition time. The density/concentration of released gaseous mixtures varies as a function of temeperature which are high at either melting or decomposition temperatures. In addition, the compound releases all types of byproducts at the decomposition temperature. Therefore, the behavior of acoustic modes

with respect to data acquisition time was measured for three compounds at their decomposition temperatures i.e. at 260, 275 and 270 ^{o}C, respectively. As we know that within short collision time, the amplitude of generated acoustic signal is high. Therefore, the PA spectra recorded at lower data acquisition times have high intensities. In PA spectra of *P*-Me-DNPT, at t = 0.5 ms, the acoustic modes at 3.8 and 27.8 kHz have almost near intensities. Similarly, the modes 3.8 and 13.8 possess identical intensities for *P*-NH_2-DNPT, while the behavior of modes for *P*-OMe-DNPT is different from one to another. This indicates that the variation in the velocity of acoustic pressure wave is due to the change in the concentration of released vapor. As a result, the predominant order and the excitation behavior of acoustic modes vary from compound to compound with respect to data acquisition time.

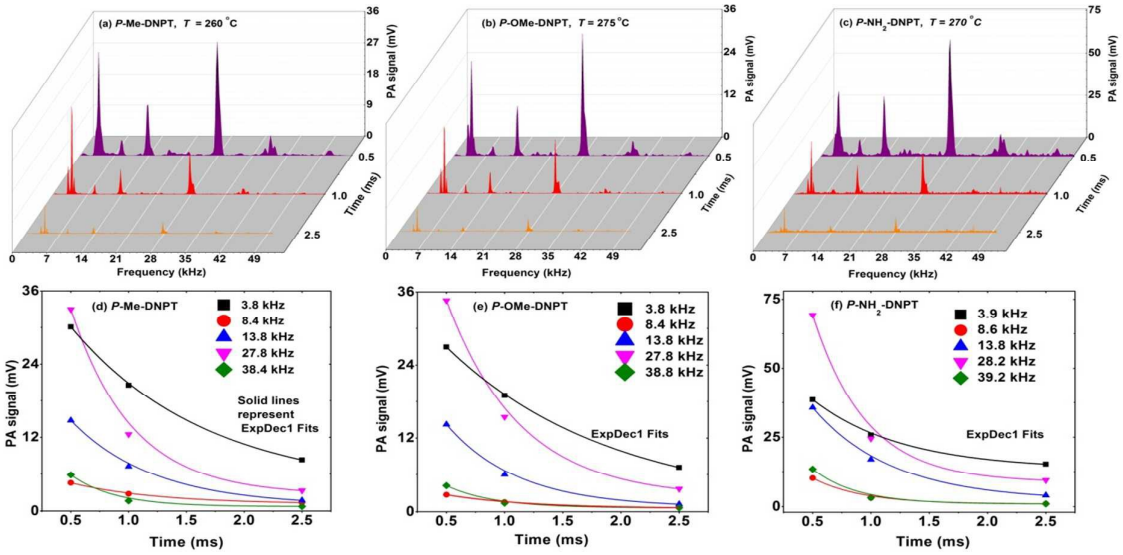

Fig. 7. (a, b and c) PA spectra and (d, e and f) behavior of acoustic modes with data acquisition time for *P*-Me-DNPT, *P*-OMe-DNPT, and *P*-NH_2-DNPT respectively.

The excited acoustic modes for all the compounds possess exponential decay behavior having different decay times (t_{non}). For all the compounds, at t= 0.5 ms ~ 28 kHz has high intensity. Further increase of data acquisition time the acoustic mode ~ 3.8 kHz replaced the

predominant position. Therefore, this mode has higher decay times compared to all other modes. The decay times of excited acoustic modes are shown in Table 4.

Table 4 Decay times of excited acoustic modes.

P-Me-DNPT	Mode (kHz)	3.8	8.4	13.8	27.8	38.4
	t_{non} (ms)	1.17	0.75	0.71	0.52	0.38
P-OMe-DNPT	Mode (kHz)	3.8	8.4	13.8	27.8	38.8
	t_{non} (ms)	1.41	0.70	0.61	0.63	0.41
P-NH_2-DNPT	Mode (kHz)	3.9	8.6	13.8	28.2	39.2
	t_{non} (ms)	0.77	0.43	0.68	0.45	0.38

3.6. *Quality factor "Q"*

The quality factor "Q" is defined by the ratio of central frequency to the full width half maximum (FWHM) of the excited acoustic mode. Fig. 8(a-c) shows the Lorentz fit of experimental data points for the acoustic mode present at ~13.8 kHz. This is one of the common acoustic mode present in PA spectra of compound and also have sharp profile. Therefore, this mode was chosen to evaluate the quality factor.

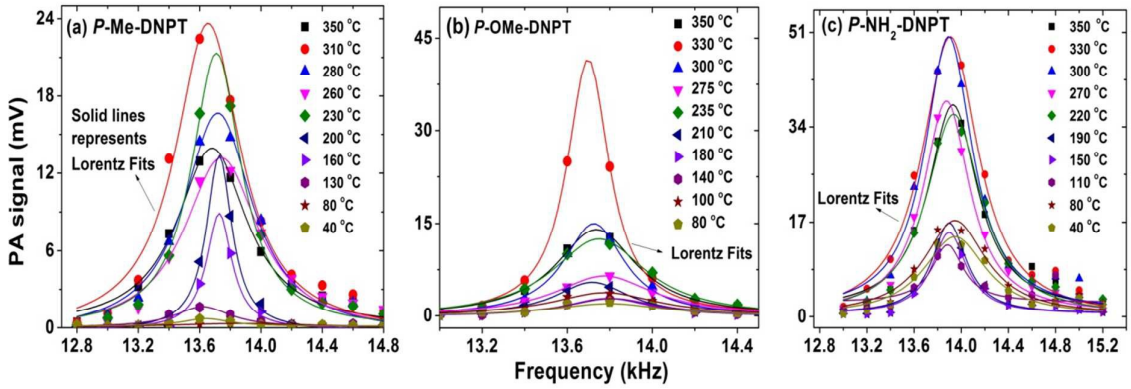

Fig. 8. Lorentz fit of acoustic modes

Fig. 8 clearly shows that the central frequency of acoustic modes do not vary with respect to vapor temperature. It confirms that the entire gaseous mixture absorbed the incident laser radiation of 266 nm wavelength and generated strong PA signal. However, in the case of

excitation wavelength 532 nm, the PA spectra is produced by thermally released NO_2 molecules and the presence of other gaseous mixtures leads to changes in the central frequency of acoustic modes [45]. The quality factors of PA cell at 13.7 kHz with respect to temperature are comprised in Table 5.

Table 5 Quality factors

Compound	Temperature and quality factor
P-Me-DNPT	*T* (°C) : 40 80 130 160 200 230 260 280 310 Q : 37 11 31 68 68 34 23 25 26
P-OMe-DNPT	*T* (°C) : 40 80 100 140 180 210 235 275 300 330 350 Q : 22 22 23 27 28 32 26 24 39 57 30
P-NH_2-DNPT	*T* (°C) : 40 80 110 150 190 220 270 300 330 350 Q : 22 22 43 39 39 25 29 28 24 27

The compound *P*-Me-DNPT has highest quality factor i.e. 68 obtained for 160 and 230 °C. While, Q: 57 achieved at 330 °C for *P*-OMe-DNPT, and Q: 43 are obtained for *P*-NH_2-DNPT. The values of quality factors listed in Table 4 reveal that individual compounds have almost identical values except at certain temperatures that have high value of quality factors. Therefore, the constant values of Q for each compounds demonstrate that their thermal stability.

The present study shows that the reported compounds are thermally stable and follows the stability order *P*-OMe-DNPT > *P*-Me-DNPT > *P*-NH_2-DNPT. However, the efficiency of these compounds as rocket fuels follows the order: *P*-NH_2-DNPT > *P*-Me-DNPT > *P*-OMe-DNPT. In our earlier report based on 532 nm wavelength it was also proved that these materials are thermally stable and efficiency of the compounds as rocket fuels follows the similar order [1]. Therefore, we are proposing that irrespective of excitation wavelength (based on different

gaseous absorption properties) using pulsed photoacoustic pyrolysis technique, we can study the thermal decomposition and stability of HEMs molecules.

4. Conclusions

We have made a successful record for the thermal PA fingerprint spectra of 1-(4-Methyl-3,5-dinitrophenyl)-1H-1,2,4-triazole (*P*-Me-DNPT), 1-(4-Methoxy-3,5-dinitrophenyl)-1H-1,2,4-triazole (*P*-OMe-DNPT), 2,6-Dinitro-4-(1H-1,2,4-triazol-1-yl) aniline (*P*-NH_2-DNPT) using Nd: YAG laser system of 266 nm wavelength of pulse duration 7 ns and repetition rate 10 Hz. The thermal decomposition mechanism and stability criteria of these compounds are explained based on the strength of PA signals and TG-DTA data. The role of chemical substituent has been studied in the comparative fingerprint spectra of the compounds. The effect of data acquisition time is studied to understand the decay behavior of acoustic modes. Thermal quality factor of the PA cavity is also measured to test the stability of the compounds. The obtained results also show that high density of compounds leads to higher strength of PA signals, which enhance the efficiency of the compounds as a rocket fuels. The efficiency of these compounds as per military application such as rocket fuel and explosives is found which follows the order of *P*-NH_2-DNPT > *P*-Me-DNPT> *P*-OMe-DNPT.

Acknowledgements:

The authors gratefully acknowledge the D.R.D.O., Ministry of Defence, Govt. of India, India, for financial support. Thanks to Dr. Kommu Nagarjuna (ACRHEM) and Dr. A. K. Sahoo (School of Chemistry, University of Hyderabad) for providing the studied samples. In addition, our sincere thanks to Dr. K.V. Rao, Director, ACRHEM, University of Hyderabad, for moral encouragement.

References

1. K. S. Rao, A. K. Chaudhary, N. Kommu, and A. K. Sahoo, *RSC Adv.*, 2016, **6**, 4053–4062.
2. Z. Rui-Zhou, L. Xiao-Hong, and Z. Xian-Zhou, *J. Chem. Sci.*, 2012, **124**, 995–1006.
3. A. Jai Prakash and H. Robert, *Organic Chemistry of Explosives*, Wiley, 2006.
4. A. K. Sikder, G. Maddala, J. P. Agrawal, and H. Singh, *J. Hazard. Mater.*, 2001, **84**, 1–26.
5. A. K. Sikder and N. Sikder, *J. Hazard. Mater.*, 2004, **112**, 1–15.
6. S. Tagomori, Y. Kuwahara, H. Masamoto, M. Shigematsu, and K. Wasana, *4th Int. Conf. Biol. Environ. Chem. IPCBEE*, 2013, **58**.
7. V. L. Korolev, T. V. Petukhova, T. S. Pivina, A. A. Porollo, A. B. Sheremetev, K. Y. Suponitskii, and V. P. Ivshinb, *Russ. Chem. Bull. Int. Ed.*, 2006, **55**, 1388–1410.
8. I. V Tselinskii, V. V Tolstyakov, S. M. Putis, and S. F. Mel, *Russ. Chem. Bull. Int. Ed.*, 2009, **58**, 2356–2361.
9. R. Tsyshevsky and M. Kuklja, *Molecules*, 2013, **18**, 8500–8517.
10. D. R. Godhani, A. A. Jogel, A. M. Sanghani, and J. P. Mehta, *J. Chem. Pharm. Res*, 2014, **6**, 1034–1041.
11. R. S. Stepanov, L. A. Kruglyakova, O. A. Golubtsova, and A. M. Astakhov, *Chem. Heterocycl. Compd.*, 2003, **39**, 604–607.
12. A. A. Dippold and T. M. Klapötke, *Chemistry*, 2012, **18**, 16742–53.
13. N. Sasidharan, B. Hariharanath, and a. G. Rajendran, *Thermochim. Acta*, 2011, **520**, 139–144.
14. D. E. G. Jones, P. D. Lightfoot, R. C. Fouchard, Q. Kwok, A. M. Turcotte, and W. Ridley, *Thermochim. Acta*, 2002, **384**, 57–69.
15. S. Mousavi and K. Esmaeilpour, *Cent. Eur. J. Energ. Mater.*, 2013, **10**, 455–465.
16. X.-R. Li and H. Koseki, *J. Loss Prev. Process Ind.*, 2005, **18**, 460–464.
17. P. G. Laye and D. C. Nelson, *Thermochim. Acta*, 1989, **153**, 221–229.
18. M. F. Foltz, C. L. Coon, F. Garcia, and A. L. Nichols III, *Propellants, Explos. Pyrotech.*, 1994, **19**, 133–144.
19. J. S. Caygill, F. Davis, and S. P. J. Higson, *Talanta*, 2012, **88**, 14–29.

20. J. Hildenbrand, J. Herbst, J. Wöllenstein, and A. Lambrecht, *Proc SPIE*, 2009, **7222**, 72220B–72220B–12.

21. R. Turcotte, M. Vachon, Q. S. M. Kwok, R. Wang, and D. E. G. Jones, *Thermochim. Acta*, 2005, **433**, 105–115.

22. Y. Q. Guo, a Bhattacharya, and E. R. Bernstein, *J. Phys. Chem. A*, 2009, **113**, 85–96.

23. *HITRAN 2014 database,online http//www.hitran.com/.*

24. K. S. Rao, A. K. Chaudhary, F. Yehya, and A. S. Kumar, *Spectrochim. Acta Part A Mol. Biomol. Spectrosc.*, 2015, **147**, 316–323.

25. A. K. Chaudhary, K. S. Rao, and A. Sudheer Kumar, *Appl. Opt.*, 2016, **55**, 817–824.

26. K. S. Rao and A. K. Chaudhary, *Thermochim. Acta*, 2015, **614**, 149–156.

27. M. S. Park, K.-H. Jung, H. P. Upadhyaya, and H.-R. Volpp, *Chem. Phys.*, 2001, **270**, 133–139.

28. A. Strachan, E. M. Kober, A. C. T. van Duin, J. Oxgaard, and W. a Goddard, *J. Chem. Phys.*, 2005, **122**, 54502:1–10.

29. A. V. Kimmel, P. V. Sushko, A. L. Shluger, and M. M. Kuklja, *J. Chem. Phys.*, 2007, **126**, 234711:1–10.

30. T. B. Ryerson, E. J. Williams, and F. C. Fehsenfeld, *J. Geophys. Res.*, 2000, **105**, 26447–26461.

31. Y. Sadanaga, Y. Fukumori, T. Kobashi, M. Nagata, and N. Takenaka, *Anal. Chem.*, 2010, **82**, 9234–9239.

32. I. During, W. Bachlin, M. Ketzel, A. Baum, U. Friedrich, and S. Wurzler, *Meteorol. Zeitschrift*, 2011, **20**, 67–73.

33. I. Barnes and K. J. Rudziński, *NATO Sci. Peace Secur. Ser. C Environ. Secur.*, 2013, **120**, 15–29.

34. E. J. Dunlea, S. C. Herndon, D. D. Nelson, R. M. Volkamer, F. San Martini, P. M. Sheehy, M. S. Zahniser, J. H. Shorter, J. C. Wormhoudt, B. K. Lamb, E. J. Allwine, J. S. Gaffney, N. a. Marley, M. Grutter, C. Marquez, S. Blanco, B. Cardenas, a. Retama, C. R. Ramos Villegas, C. E. Kolb, L. T. Molina, and M. J. Molina, *Atmos. Chem. Phys.*, 2007, **7**, 2691–2704.

35. C. T. Dinh, S. Hoogland, and E. H. Sargent, *Ind. Eng. Chem. Res.*, 2015, **54**, 12750–12756.

36. N. Kommu, V. D. Ghule, A. S. Kumar, and A. K. Sahoo, *Chem. - An Asian J.*, 2014, **9**, 166–178.

37. F. Yehya and A. K. Chaudhary, *Sensors Actuators B. Chem.*, 2013, **178**, 324–330.

38. F. Yehya, A. K. Chaudhary, D. Srinivas, and K. Muralidharan, *Appl. Phys. B*, 2015, **121**, 193–202.

39. Q. Zhao, S. Zhang, and Q. S. Li, *Chem. Phys. Lett.*, 2005, **407**, 105–109.

40. J. S. Murray and P. Politzer, in *Chemistry and Physics of Energetic Materials SE - 8*, ed. S. Bulusu, Springer Netherlands, 1990, vol. 309, pp. 157–173.

41. S. Zhang and T. N. Truong, *J. Phys. Chem. A*, 2000, **104**, 7304–7307.

42. J. S. Boyer, *Nitrozoles*, (Deerfield Beach: VCH Publishers), 1986.

43. N. Kommu, V. D. Ghule, a. S. Kumar, and A. K. Sahoo, *Chem. - An Asian J.*, 2014, **9**, 166–178.

44. T. Fendt, N. Fischer, T. M. Klapötke, and J. Stierstorfer, *Inorg. Chem.*, 2011, **50**, 1447–1458.

45. K. S. Rao, A. K. Chaudhary, and F. Yehya, *Appl. Phys. B*, 2015, **121**, 375–384.